RSC Advances

ROYAL SOCIETY OF CHEMISTRY

www.rsc.org/advances

Mechanistic study of selective catalytic reduction of NO with NH_3 over highly dispersed Fe_2O_3 loaded on Fe-ZSM-5

Bo Li [1], Zhennan Huang [2], Xiaodong Huang [1], Shengzhong Kou [2], Fu Liu [1], Xiaobin Zhang [1], Hangsheng Yang [1*]

[1] *State Key Laboratory of Silicon Materials, School of Materials Science and Engineering, Zhejiang University, Zheda Road 38, Hangzhou 310027, China*

[2] *State Key Laboratory of Advanced Processing and Recycling of Nonferrous Metals, Lanzhou University of Technology, Lanzhou 730050, China*

[*]To whom correspondence should be addressed. Tel/Fax: +86-571-87951404; E-mail: hsyang@zju.edu.cn

Abstract: ZSM-5 supported highly dispersed Fe_xO_y clusters was prepared by sol-gel method for selective catalytic reduction (SCR) of NO with NH_3. XRD, SEM, UV-vis, H_2-temperature-programmed reduction (H_2-TPR), NH_3-temperature-programmed desorption (NH_3-TPD), and BET analyses all indicated that Fe species mainly existed as highly dispersed surface Fe_xO_y clusters with a Fe^{3+} concentration of 22 wt%. NO-Temperature-programmed oxidation (NO-TPO) revealed that the Fe_xO_y clusters promoted the oxidation of NO to NO_2, which promoted the low temperature NO_X removal. NH_3 was activated above 250 °C and over oxidation of NH_3 to NO_X was not observed, as a result, a NO_X removal efficiency of 91% was achieved at 400 °C. Moreover, the SCR reaction route was found to be temperature dependent, below 200 °C, the NO_X reduction followed the reaction between NO_2 and non-activated NH_3. Fast SCR reaction dominated the NO_X removal at the temperature window of 200-325 °C. At temperature above 250 °C, the normal reaction between activated NH_3 and NO compensated the thermodynamic limitation induced suppression of fast SCR.

Keywords: Selective catalytic reduction; Fe-ZSM-5; Fe_xO_y clusters; NO_X; fast SCR

1. Introduction

Many industrial processes use nitrogen oxides (NO_X, mainly NO and NO_2) containing reactants or produce NO_X as by-products, especially in the exhaust gases, which remain a major source for air pollution. In fact, NO_X have given rise to a variety of increasingly harmful impacts on the environment, such as photochemical smog, acid rain, ozone depletion and greenhouse effects. Due to the increasing threat of NO_X to the environment, a great many approaches have been developed to try to control its emission. Among them, selective catalytic reduction (SCR), using V_2O_5 as active catalyst and NH_3 as reductant, has been proven to be the most effective technology and has been widely applied to reduce the NO_X emission from power plants and waste incinerations [1-4]. As a widely used catalyst, the detrimental of V_2O_5-based catalyst is its high toxicity, high activity for SO_2 oxidation, formation of N_2O at high temperature, which stimulated the continuing efforts to develop new catalysts [5-14]. Recently, zeolite based catalysts have attracted much interest for the reduction of NO to N_2 by NH_3, because of their remarkable catalytic activity and nontoxic, lower activity for the oxidation of SO_2 to SO_3, and low N_2O by-product [15-22]. Among them, Fe-exchanged/loaded ZSM-5 showed high activities for the SCR reaction of NO_X by NH_3 [9]. It was reported that even under the condition of very low iron loading, a moderate activity could be achieved over Fe-ZSM-5 [23]. Especially heavy/over loaded Fe-ZSM-5 showed a high NO reduction activity and stability in SO_2 and H_2O, even higher than that of commercial V_2O_5-based catalysts [9, 24, 25]. And the combination of the NH_3 adsorption by zeolite and oxidation of NO to

NO_2 by Fe^{3+} was considered to be responsible for its high performance [26, 27].

From literature, the activity was found to be enhanced by increasing the amount of the Fe^{3+} exchanged/loaded on ZSM-5; however, the preparation of heavy exchange Fe-ZSM-5 with Fe concentration above 2% is still a challenge [9]. In this study, by conventional aqueous ion-exchange technique using $FeCl_2$ as reactant [28], we found that highly dispersed Fe_xO_y clusters with a Fe^{3+} concentration of 22 wt% was successfully loaded on Fe-ZSM-5, which further promoted de-NO_X activity and broadened the reaction temperature window from 250 °C to 400 °C. Our results also suggest that the reaction route for SCR of NO_X is reaction temperature dependent, at least over Fe-ZSM-5 supported highly dispersed Fe_xO_y clusters.

2. Experimental

2.1 Catalyst preparation

The starting zeolite was H-ZSM-5 (Nankai University, Si/Al ≈ 25, S_{BET} = 425 m^2/g). $FeCl_2$ (99 wt%, Aldrich) was used as Fe precursors. Fe-ZSM-5 was prepared using a conventional aqueous ion-exchange technique [28]. 10 grams of H-ZSM-5 was added to 1 L of 0.05 M $FeCl_2$ solution with constant stirring in air for 24 h, after stirring, the pH of the solution was measured to be 4, which facilitate the Fe ions exchange into ZSM-5 and Fe_xO_y dispersion [29]. For normal Fe-ZSM-5, the mixture was filtered and thoroughly washed with deionized water and then dried at 90 °C for 10 h. For Fe_xO_y clusters heavy loaded zeolite (Fe_H-ZSM-5), the mixture was dried at 90 °C directly without washing. The obtained samples were then calcined at 500 °C

for 6 h in air. For comparison, pure Fe_2O_3 was prepared by the same procedure without H-ZSM-5. Details of the surface element composition and structure properties of catalysts were summarized in Table 1.

2.2 Catalyst characterization

X-ray diffraction (XRD) patterns were recorded on a Philips XD-98 X-ray diffractometer using Cu Kα radiation (k = 0.15406 nm). Brunauer-Emmett-Teller (BET) surface areas were studied using an ASAP2000 physical absorber. The morphology was characterized by scanning electron microscopy (SEM) (JEOL S-4800); energy dispersive spectrometry (EDS) was carried out in the same facility. X-ray photoelectron spectroscopic (XPS) data were obtained using a Thermo ESCALAB 250, the X-ray source was an Al Kα radiation, and all binding energies were referenced to the 284.8 eV C 1s.

The UV-vis diffuse reflection spectra were obtained for the dry-pressed disk samples using a Scan UV-vis spectrophotometer (UV-vis DRS: TU-1901, China) equipped with an integrating sphere assembly, and $BaSO_4$ as reflectance sample. The spectra were recorded at room temperature in air ranged from 200 to 800 nm. All the samples were degassed at 200 °C prior to measurements.

H_2-temperature-programmed reduction (H_2-TPR) experiments were performed using 100 mg of each catalyst. The catalysts were preheated at 400 °C for 1 h in air. After they were cooled to 100 °C, the samples were heated up to 800 °C with a heating rate of 10 °C/min under a mixed flow of 10% H_2 in helium and a flow rate of 30 mL/min.

NH_3-temperature-programmed desorption (NH_3-TPD) experiments were performed using 100 mg of each catalyst to determine their NH_3 adsorption. The sample was preheated in a N_2 stream (30 mL/min) at 400 °C for 1 h, and then cooled to 100 °C. The pretreated sample was then exposed to a mixed flow of 4% NH_3 in argon at a flow rate of 20 mL/min for 3 h at 100 °C, and heated up to 800 °C at a heating rate of 10 °C/min. The H_2-TPR and NH_3-TPD data were recorded using an on-line gas chromatograph equipped with a thermal conductivity detector.

NO-temperature-programmed desorption (NO-TPD) experiments were performed in a fixed-bed flow reactor. 1.5 g of each catalyst was pasted on three Al plates and inserted into the fixed-bed [30]. The samples were exposed to a 800 ppm NO flow without O_2 for 1 h at 400 °C and cooled to 100 °C in the same gas stream, then the samples were purged by a N_2 until the NO signal returned to the baseline level. Finally, the temperature was ramped from 80 °C to 400 °C in N_2 at a heating rate of 10 °C/min. Similarly, NO_2-TPD experiments were performance in 800 ppm NO_2 diluted in N_2 without O_2. And the desorbed NO/NO_2 concentrations depended on temperature were recorded using an NO-NO_2-NO_X analyzer (Testo AG testo 340).

NO-temperature-programmed oxidation (NO-TPO) experiments were performed in the same reactor from 100 °C to 400 °C under 800 ppm of NO, 5% O_2 and a N_2 balance at a total flow rate of 1000 sccm. NH_3-temperature-programmed oxidation (NH_3-TPO) experiments were also performed in the same fixed-bed flow reactor from under from 100 °C to 400 °C in 800 ppm NH_3, 5% O_2, and a N_2 balance at a total flow rate of 1000 sccm. The inlet and outlet concentrations of NH_3 were determined

by titration with 0.001 M hydrochloric acid, and methyl red was used as the indicator.

2.3 Catalyst activity characterization

The catalytic activity tests were carried out in a fixed-bed quartz reactor with 1.5 g catalyst pasted on three Al plates (4 cm × 10 cm) [30]. The inlet and outlet concentrations of NO and NO_2 were monitored using Testo AG testo 340. The simulated gas used for these tests contained 800 ppm NO, 800 ppm NH_3 and 5 vol% O_2 balanced by N_2 at total flow rate of 1000 sccm and a GHSV of 100,000 h^{-1}.

3 Results and discussion

3.1 Catalyst activity

Figure 1 shows NO_X conversion as a function of temperature over different catalysts. The H-ZSM-5 catalyst presented the lowest activity for NO_X reduction in the investigated temperature window. Fe_2O_3 started to catalyze NO_X reduction at 200 °C, and the conversion increased with temperature up to 62% at 350 °C, and then fell to 38% at 400 °C. For Fe-ZSM-5, the reduction of NO_X started at 250 °C and then increased quickly and reached to 77% at 400 °C [23]. The best performance was achieved over Fe_H-ZSM-5, which showed high performance even at temperature as low as 250 °C and a NO_X conversion of 91% was achieved at 400 °C. Moreover, the activity loss at high temperature above 350 °C over normal catalysts was not observed at 400 °C.

In order to further clarify the temperature dependency of NO_X conversion, the kinetic parameters were calculated based on the assumption that the reaction is

first-order dependent on NO and zero-order dependent on NH_3, and the kinetic parameters were calculated from NO conversion over Fe_H-ZSM-5 as [31-33]:

$$k = -\frac{V}{M} \cdot \ln(1 - x) \quad (1)$$

$$k = k_0 \cdot \exp\left(\frac{-Ea}{RT}\right) \quad (2)$$

where k is the reaction rate coefficient (mL g^{-1} s^{-1}), V is the total gas flow rate (mL s^{-1}), M is the catalyst weight (g), x is the conversion of NO_X (%).The obtained values of k were used in the Arrhenius plot and then the activation energies (E_a) of the SCR reaction were derived .

As shown in Fig. 1b, the reaction can be divided into three stages, at temperature below 200 °C, the apparent E_a was calculated as low as 8.98 kJ/mol; the highest E_a of 27.01 kJ/mol was calculated at temperature between 200 and 325 °C; at temperature above 325 °C, the E_a was calculated to be 10.78 kJ/mol. This suggests that the reaction route for NO reduction is temperature dependent.

3.2 XRD, SEM and BET study

The crystallographic structures of the ZSM-5 support and Fe-ZSM-5 zeolite were studied by XRD as shown in Fig. 2. All of the XRD patterns showed three diffraction peaks at 2θ = 23-25°, matching well with the standard phase of ZSM-5 zeolite [34], indicating that the frame structure of ZSM-5 was not destroyed during Fe^{3+} ions exchanging and/or Fe_xO_y clusters loaded. The spectrum of H-ZSM-5 are same as that of Fe-ZSM-5, indicating Fe^{3+} occupied the H^+ position [35]. Pure Fe_2O_3 existed as

α-Fe_2O_3 which was supported by the diffraction peaks at 33.1°, 35.6°, 40.9°, 49.5°, and 54.1°. While for Fe_H-ZSM-5, peaks attributed to Fe_2O_3 were not detected obviously, indicates a high dispersion of Fe_xO_y clusters on Fe-ZSM-5 [36].

Fig. 3 shows typical SEM images of samples, Fe_2O_3 showed typical needle like morphology, suggesting the α-Fe_2O_3 structure [37], three zeolite containing samples showed very similar morphology, again indicating the fact that frame structure was remained during Fe^{3+} ions exchanging and/or Fe_xO_y clusters loaded. The needle like Fe_2O_3 phase was not observed by SEM observation in Fe_H-ZSM-5, further proved the high dispersion of Fe_xO_y clusters. This assumption was also supported by BET measurement as shown in Table 1, after Fe^{3+} was exchanged into zeolite to form Fe-ZSM-5, the surface area decreased from 425 to 391 m^2/g, in agreement with other reports [38]. The surface area of Fe_H-ZSM-5 reduced to 305.65 m^2/g due to the loading of Fe_xO_y clusters. From the pore size change caused by Fe^{3+} exchange and Fe_xO_y clusters loading (from 1.162 nm to 1.13 nm and 1.08 nm for Fe-ZSM-5 and Fe_H-ZSM-5), Fe^{3+} substituted the H^+, at the same time Fe_xO_y clusters also loaded inside the micropores of zeolite, thus reduced the pore size of Fe_H-ZSM-5.

3.3 UV-vis analysis

The UV-vis spectra were shown in Fig. 4. The UV-vis spectra of Fe-ZSM-5 and Fe_H-ZSM-5 zeolites presented in this work have been deconvoluted into subbands to facilitate the assignment of different Fe species, detailed information was shown in Table 2. For Fe-ZSM-5, two strong peaks located at 218 nm and 270 nm could be

attributed to the isolated Fe^{3+} sites in tetrahedral and higher coordination (five or six oxygen ligands) [39-41], the peaks located at 300-400 nm (assigned to oligomeric clusters) and > 400 nm (assigned to large Fe_2O_3 clusters) were weak [39-41]. This indicated that Fe species were mainly exchanged into zeolite to form Fe-ZSM-5. While for Fe_H-ZSM-5, besides the peaks attributed to isolated Fe^{3+}, peaks for Fe_xO_y clusters were also strong, which indicated that Fe^{3+} species mainly loaded on the zeolite surface as clusters with good dispersion, in good agreement with our XRD measurements. In fact, the XRD peaks attributed to Fe_2O_3 were hardly detected. As shown in Table 2, semi-quantitative analysis revealed that more than 60% of the Fe^{3+} species were exchanged into zeolite in Fe-ZSM-5, and more than 70% of Fe^{3+} species existed as Fe_xO_y clusters in Fe_H-ZSM-5.

3.4 XPS analysis

The XPS results were shown in Fig. 5, for Fe_2O_3, the binding energies of $Fe_{2p3/2}$ and $Fe_{2p1/2}$ in Fig. 5 are located around 711.2 and 725.5 eV, indicating that Fe is directly bonded to O [42]. Both $Fe_{2p3/2}$ and $Fe_{2p1/2}$ peaks are accompanied by a small satellite on the high binding energy side, which is the characteristic of Fe^{3+} in Fe_2O_3, in consistent with XRD characterization [43]. According to Jin's report [42], when the calcine temperature was >500 °C, Fe^{3+} became the main products in Fe-ZSM-5. Here the Fe related peaks in Fe-ZSM-5 is very weak, only a small difference can be observed as the inset shown, indicating a low Fe exchange in Fe-ZSM-5 after water washing. While for Fe_H-ZSM-5, Fe related peaks were evident and all the iron species

existed as Fe^{3+}.

3.5 H_2-TPR and NH_3-TPD analysis

H_2-TPR experiments were shown in Fig. 6. H-ZSM-5 had no obvious H_2 consumption peaks during the whole temperature range, indicating that the ZSM-5 zeolite support shows no oxidation ability. Fe_2O_3 showed an obvious reduction peak around 370 °C and another large broad peak around 660 °C, which are attributed to the reduction from Fe_2O_3 to Fe_3O_4, and the overlap of Fe_3O_4 to FeO and Fe, respectively [44]. Due to the low Fe loading in Fe-ZSM-5, the Fe related reduction peaks could hardly detect, with very weak peak around 350 °C. In the case of Fe_H-ZSM-5, the peak attributed to Fe_2O_3 to Fe_3O_4 reduction disappeared, and a new peak located between 400 and 500 °C was detected, moreover, the peaks attributed to Fe_3O_4 to FeO and FeO to Fe was separated. Similar phenomena was also reported by Heinrich and Chen [45, 46], normally, the reduction peak is expected to shift to the low temperature side due to the high dispersion of Fe_xO_y clusters, however, the delayed water removal from the surrounding microporous network structure induced the peak to shifted to the high temperature side [45, 46]. Also, the existence of interaction between highly dispersed Fe_xO_y clusters and zeolite could further shift the peak to higher temperature [47].

The NH_3-TPD results are shown in Fig. 7. All the ZSM-5 profiles display two peaks centered at about 180 °C and 340 °C, ascribed to weak and strong surface acid sites [48, 49]. While for Fe_2O_3, only a strong peak around 220 °C was observed, no strong acid site in Fe_2O_3 indicating that it did not absorb NH_3 at temperature above

300 °C. The area of the subbands of the TPD spectra were calculated and shown in Table 2. The NH_3 desorption peak at 180 °C and 340 °C over Fe-ZSM-5 and Fe_H-ZSM-5 was less than that over H-ZSM-5, which suggested that part of the Fe^{3+} occupied H^+ site and Fe_xO_y clusters further covered parts of surface H^+ in zeolite (the surface H^+ is considered to be the origin of the strong acid sites [50, 51]), thus reduced the NH_3 adsorption capacity of Fe_H-ZSM-5 even less than Fe-ZSM-5, in agreement with our TPR and BET analyses.

3.6 NO to NO_2 oxidation and NO_X TPD

According to literature [13, 52], the existence of NO_2 can accelerate the SCR reaction. Therefore, the NO to NO_2 oxidation as a function of reaction temperature was studied and shown in Fig. 8. Both H-ZSM-5 and Fe_2O_3 showed very low activity for NO to NO_2 oxidation. NO_X conversion kept below 25% through the whole temperature range, while the Fe-ZSM-5 showed relative high activity and NO oxidation reached the maximum of 53% at 325 °C. Then the NO oxidation efficiency decreased with further increasing the temperature due to the thermodynamic limits [52]. These results suggest that Fe-ZSM-5 has better catalytic activity to promote NO oxidation ability than Fe_2O_3, and thus accelerate the SCR reaction remarkable. The performance of Fe_H-ZSM-5 is very similar to that of Fe-ZSM-5, but it showed a higher activity at low temperature side, which could be attributed to the highly dispersed Fe_xO_y clusters in Fe_H-ZSM-5.

According to Fig. 8, the apparent E_a for NO oxidation over Fe_H-ZSM-5 and

Fe-ZSM-5 was calculated to be 13.35 and 24.98 kJ/mol, respectively. Note that the apparent E_a of NO oxidation over Fe_H-ZSM-5 was close to the E_a of NO_x reduction at temperature below 200 °C (8.98 kJ/mol), which suggests that the NO oxidation played an important role in the rate-determining step during NO reduction below 200 °C.

Adsorption of NO_X species on the catalyst surface was reported to play an important role in NO_X reduction [53]. Fig. 9 shows the NO_X desorption profiles of this series of catalysts. Fe_2O_3 is good adsorbent for both NO and NO_2, and H-ZSM-5 is not a good adsorbent for either NO or NO_2. Fe-ZSM-5 only adsorbed NO_2, moreover, Fe_H-ZSM-5 was also found to adsorb NO_2 only, which strongly suggested the existence of interaction between highly dispersed Fe_xO_y clusters and zeolite supporter.

3.7 NH_3 Oxidation analysis

In SCR reaction, ammonia activation is considered as one of the most important parameters to promote the NO_X conversion, especially over traditional V_2O_5-based catalysts [54]. Fig. 10 shows the NH_3 oxidation over this series of catalysts. NH_3 conversion over all the catalysts kept at almost 0% below 225 °C. Then NH_3 conversion increased with temperature. H-ZSM-5 showed low activity for NH_3 oxidation even at high temperature. The Fe-ZSM-5 catalyst only showed a limited activity promotion compared to H-ZSM-5 due to the low Fe^{3+} loading. Interestingly, the NH_3 oxidation over Fe_H-ZSM-5 was found to be higher than that over pure Fe_2O_3

and reached 56% at 400 °C, indicating that highly dispersed Fe_xO_y clusters promoted the NH_3 activation, since the Fe_H-ZSM-5 performed better than Fe-ZSM-5 which has the same amount of Fe exchanged in ZSM-5, and even better than pure Fe_2O_3. Furthermore, during NH_3 oxidation, NO or NO_2 species was not detected over all catalysts, indicating no NH_3 over oxidation, which should be beneficial for SCR NO_X removal at high temperature.

3.8 Discussions

Fe-ZSM-5 has been widely studied as catalyst for the ammonia SCR reaction. The Fe species in Fe-ZSM-5 were partly exchanged into zeolite, and partly loaded on the zeolite surface as clusters [39-41]. On the one hand, Fe in Fe-ZSM-5 was reported to promote the oxidation of NO to NO_2. On the other hand, the loaded Fe ions replaced the H^+, which caused the slightly decrease of NH_3 adsorption [26, 55]. Fortunately, the reaction between NO and O_2, but not the NH_3 adsorption, was considered as the rate-determining step [56]. As a result, Fe-ZSM-5 promoted the NO_X reduction. This is supported by another report which found that the SCR activity of Fe-ZSM-5 is tremendously improved by the addition of NO_2 to the feed gas, especially at low reaction temperature [52]. Further study suggested that the role of NO_2 in the fast SCR reaction was to form surface nitrites and nitrates, while the role of NO is to reduce nitrates to nitrites, and then nitrates further reacted with NO to produce more nitrides, finally nitrites were removed from the surface by NH_3 to produce N_2, the reduction of nitrates by NO is the rate-limiting step in this fast SCR at

200 °C [57]. While at high temperature above 300 °C, the NO_X conversion in SCR reaction is mainly governed by ammonia activation since the NO oxidation is suppressed due to the thermodynamic limitation. However the undesirable over oxidation of NH_3 to NO_X occurred easily at high temperature [54, 58, 59].

In the present study, according to NO_X TPD and NO oxidation results, H-ZSM-5 showed no ability for either NO to NO_2 oxidation or NO + NO_2 adsorption, so NO_X conversion could not happen over H-ZSM-5 at low temperature. At temperature above 350 °C, H-ZSM-5 started to activate NH_3 as shown in Figs. 7 and 10, and this promoted NO_X reduction and a NO_X conversion up to 15% was obtained. For, Fe-ZSM-5, it started to reduce NO at 150 °C and the reduction increased quickly at temperature above 250 °C, which is in good agreement with the NO oxidation and adsorption as shown in Figs. 8 and 9 [13, 52]. Note that the Fe^{3+} concentration is low in Fe-ZSM-5, which indicated that the isolated Fe^{3+} sites in tetrahedral and higher coordination are excellent active species for NO_X reduction. At temperature above 325 °C, the NO to NO_2 oxidation were reduced due to the thermodynamic limit [52], and NO_2 adsorption also reduced, however, the NO_X reduction still increased, which could be attributed to the NH_3 activation at high temperature as shown in Figs. 7 and 10.

For Fe_2O_3, the oxidation of NO to NO_2 was poor, even poorer than that of H-ZSM-5, but it adsorbed NO and NO_2 as shown in Fig. 9, and it also activated the NH_3 above 250 °C, which enhanced the NO_X reduction up to 62% at 350 °C, at temperature above 350 °C, NO and NO_2 adsorptions were suppressed, and NH_3 was

also totally desorbed (Fig. 7), which finally decreased the NO_X reduction.

The detrimental of the Fe-ZSM-5 is its low Fe^{3+} concentration (less than 2% [9]), fortunately the surface loaded Fe_xO_y clusters are also active species, and thus in the case of Fe_H-ZSM-5, the catalyst showed 20% of NO oxidation even at 100 °C (Fig. 8), this promoted its activity and a NO_X conversion of 20% was achieved at 100 °C. In fact, as shown in Fig. 4, more than 70% of Fe species existed as surface Fe_xO_y clusters. At temperature above 350 °C, though the NO_2 adsorption and NO to NO_2 oxidation was suppressed, but this was compensated by the promotion NH_3 activation benefited from Fe_xO_y clusters as shown in Fig. 10, which still promoted the NO_X reduction, and a NO_X conversion of 91% was achieved at 400 °C.

From the view of SCR reactions, NO_2 is involved in the following reactions:

$$6NO_2 + 8NH_3 \rightarrow 7N_2 + 12H_2O \quad (1)$$

$$2NO_2 + 4NH_3 + O_2 \rightarrow 3N_2 + 6H_2O \quad (2)$$

$$2NO + 2NO_2 + 4NH_3 \rightarrow 4N_2 + 6H_2O \quad (3)$$

Among them, reaction (3) is the well-known fast SCR, while in reactions (1) and (2), NO does not react with NH_3 directly, thus the E_a would be less than that of the reaction (3) in which NO was involved. Taken the catalyst Fe_H-ZSM-5 as an example, from Figs. 1a and 8, we can find that the NO_X removal efficiency is almost the same as the NO to NO_2 oxidation below 200 °C, which suggested that NO_X removal mainly follows reactions (1) and/or (2). At temperature between 200 and 325 °C, the NO_X removal efficiency is approximately twice as that of the NO to NO_2 oxidation, indicating that reaction (3) becomes the main route. At temperature above 250°C,

NH_3 activation become notable. Therefore, the SCR reaction can be divided into three stages here: In Stage-1 (<200 °C), the main reaction is between NO_2 and non-activated NH_3; in Stage-2 (200-325 °C), the main reaction is NO + NO_2 and non-activated NH_3; while in Stage-3 (>300 °C), the reaction between NO + NO_2 and activated NH_3 becomes the main route, and the reaction between NO and activated NH_3 also occurred considering from the difference between NO to NO_2 oxidation and the NO removal efficiency. Accordingly, the lowest E_a was needed in Stage-1, and the highest E_a was needed in Stage-2, in good agreement with our E_a calculation in Fig. 1b.

4 Conclusions

In summary, highly dispersed Fe_xO_y clusters with a Fe^{3+} concentration of 22 wt% was successfully loaded on ZSM-5, the Fe_xO_y clusters played a key role for the promotion of de-NO_X activity, and a good NO_X removal efficiency of 91% was achieved at 400 °C. Our results discovered that the NO to NO_2 oxidation is essential for NO_X removal at temperature below 200 °C. At temperature between 200 °C and 325 °C, fast SCR reaction became the main route for NO_X reduction. The NH_3 activation at temperature above 300 °C promoted the reaction between NO and NH_3, which compensated thermodynamic limitation induced suppression of fast SCR. And the suppression of NH_3 to NO over oxidation promised a high NO reduction efficiency at 400 °C.

Acknowledgments: This work was supported by the Environmentally Sustainable Management of Medical Wastes in China (Contract No. C/V/S/10/251), and the National Natural Foundation of Zhejiang Province, China (Grant No. Z4080070).

Reference:

[1]. F.C. Meunier, J.P. Breen, V. Zuzaniuk, M. Olsson, J.R.H. Ross, J. Catal. 187 (1999) 493-505.

[2]. G. Busca, L. Lietti, G. Ramis, F. Berti, Appl. Catal. B: Environ. 18 (1998) 1-36.

[3]. G. Busca, M.A. Larrubia, L. Arrighi, G. Ramis, Catal. Today 107-108 (2005) 139-148.

[4]. G. Ramis, L. Yi, G. Busca, Catal. Today 28 (1996) 373-380.

[5]. Z.H. Lian, F.D. Liu, H. He, Catal. Sci. Technol. 5 (2015) 389-396.

[6]. S.W. Choi, S.K. Choi, H.K. Bae, J. Air Waste Manage. Assoc. 65 (2015) 485-491.

[7]. A. Yamamoto, Y. Mizuno, K. Teramura, S. Hosokawa, T. Shishido, T. Tanaka, Catal. Sci. Technol. 5 (2015) 556-561.

[8]. X.Y. Fan, F.M. Qiu, H.S. Yang, W. Tian, T.F. Hou, X.B. Zhang, Catal. Commun. 12 (2011) 1298-1301.

[9]. R.Q. Long, R.T. Yang, J. Catal. 188 (1999) 332-339.

[10]. Z.X. Ma, H.S. Yang, F. Liu, X.B. Zhang, Appl. Catal. A: Gen. 467 (2013) 450-455.

[11]. Z.X. Ma, H.S. Yang, Q. Li, J.W. Zheng, X.B. Zhang, Appl. Catal. A: Gen. 427-428 (2012) 43-48.

[12]. Q. Li, X.X. Hou, H.S. Yang, Z.X. Ma, J.W. Zheng, F. Liu, X.B. Zhang, Z.Y. Yuan, J. Mol. Catal. A: Chem. 356 (2012) 121-127.

[13]. Q. Li, H.S. Yang, F.M. Qiu, X.B. Zhang, J. Hazard. Mater. 192 (2011) 915-921.

[14]. W. Tian, H.S. Yang, X.Y. Fan, X.B. Zhang, J. Hazard. Mater. 188 (2011) 105-109.

[15]. R.Q. Long, R.T. Yang, R. Chang, Chem. Commun. 5 (2002) 452-453.

[16]. R.Q. Long, R.T. Yang, J. Catal. 201 (2001) 145-152.

[17]. K. Krishna, M. Makkee, Catal. Today 114 (2006) 23-30.

[18]. S. Brandenberger, O. Kröcher, A. Tissler, R. Althoff, Catal. Rev. 50 (2009) 492-531.

[19]. P.S. Metkar, V. Balakotaiah, M.P. Harold, Catal. Today 184 (2012) 115-128.

[20]. E. Kolobova, A. Pestryakov, A. Shemeryankina, Y. Kotolevich, O. Martynyuk, H.J.T. Vazquez, N. Bogdanchikova, Fuel 138 (2014) 65-71.

[21]. A. Sultana, T. Nanba, M. Haneda, H. Hamada, Catal. Commun. 10 (2009) 1859-1863.

[22]. H. Sjövall, R.J. Blint, L. Olsson, Appl. Catal. B: Environ. 92 (2009) 138-153.

[23]. A. UddOn, T. Komatsu, T. Yashima, J. Chem. Soc. Faraday Trans. 91 (1995) 3275-3279.

[24]. A.Z. Ma, W. Grünert, Chem. Commun. (1999) 71-72.

[25]. H.Y. Chen, T. Voskoboinikov, W.M.H. Sachtler, J. Catal. 180 (1998) 171-183.

[26]. R.Q. Long, R.T. Yang, J. Catal. 207 (2002) 224-231.

[27]. V.V. Lissianski, P.M. Maly, V.M. Zamansky, Ind. Eng. Chem. Res. 40 (2001) 3287-3293.

[28]. G. Qi, R.T. Yang, Catal. Lett. 100 (2005) 243-246.

[29]. J.A.Z. Pieterse, S. Booneveld, R.W. van den Brink, Appl. Catal. B: Environ. 51

(2004) 215–228

[30]. Q. Li, H.S. Yang, A.M. Nie, X.Y. Fan, X.B. Zhang, Catal. Lett. 141 (2011) 1237-1242.

[31]. J.H. Goo, M.F. Irfan, S.D. Kim, S.C. Hong, Chemosphere 67 (2007) 718-723.

[32]. X.Y. Guo, C. Bartholomew, W. Hecker, L.L. Baxter, Appl. Catal. B: Environ. 92 (2009) 30-40.

[33]. D.S. Zhou, Z.Y. Ren, B. Li, Z.X. Ma, X.B. Zhang, H.S. Yang, RSC Adv. 40 (2015) 31708-31715.

[34]. M.M.J. Treacy, J.B. Higgins, Elsevier 1996.

[35]. A. Cihanoglu, G. Gündüz, M. Dükkancı, Appl. Catal. B: Environ. 165 (2015) 687-699.

[36]. M. Rauscher, K. Kesore, R. MoÈnnig, W. Schwieger, A. Tiûler, T. Turek, App. Catal. A: Gen. 184 (1999) 249-256.

[37]. G. Huo, X.G. Lu, Y. Huang, W.Y. Li, and G.Y. Liang, J. Electrochem. Soc. 161 (2014) 1144-1148.

[38]. B.M. Reddy, K.N. Rao, G.K. Reddy, A. Khan, S.E. Park, J. Phys. Chem. C 111 (2007) 18751-18758.

[39]. S. Bordiga, R. Buzzoni, F. Geobaldo, C. Lamberti, E. Giamello, A. Zecchina, G. Leofanti, G. Petrini, G. Tozzola, G. Vlaic, J. Catal. 158 (1996) 486-501.

[40]. G. Lehmann, Z. Phys. Chem. Neue Folge. 72 (1970) 279.

[41]. M. Santhosh Kumar, M. Schwidder, W. Grünert, A. Brückner, J. Catal. 227 (2004) 384–397.

[42]. M.M. Jin, R.G. Yang, M.F. Zhao, G.Y. Li, C.W. Hu, Ind. Eng. Chem. Res. 53 (2014) 2932-2939.

[43]. J.A. Botas, J.A. Melero, F. Martınez, M.I. Pariente, Catal. Today 149 (2010) 334-340.

[44]. F.D. Liu, H. He, C.B. Zhang, Z.C. Feng, L.R. Zheng, Y.N. Xie, T.D. Hu, Appl. Catal. B: Environ. 96 (2010) 408-420.

[45]. F. Heinrich, C. Schmidt, E. Löffler, M. Menzel, W. Grünert, J. Catal. 212 (2002) 157–172.

[46]. H.Y. Chen, W.M.H. Sachtler, Catal. Today 42 (1998) 73-83.

[47]. H.L. Huang, Y. Lan, W.P. Shan, F.H. Qi, S.C. Xiong, Y. Liao, Y.W. Fu, S.J. Yang, Catal. Lett. 144 (2014) 578-584.

[48]. T. Miyamoto, N. Katada, J.H. Kim, M. Niwa, J. Phys. Chem. B 102 (1998) 6738-6745.

[49]. Y.M. Ni, A.M. Sun, X.L. Wu, G.L. Hai, J.L. Hu, T. Li, G.X. Li, Microporous Mesoporous Mater. 143 (2011) 435-442.

[50]. Y.H. Seo, E.A. Prasetyanto, N.Z. Jiang, S.M. Oh, S.E. Park, Microporous Mesoporous Mater. 128 (2010) 108-114.

[51]. G. Qi, R.T. Yang, Appl. Catal. B: Environ. 60 (2005) 13-22.

[52]. M. Devadas, O. Kröcher, M. Elsener, A. Wokaun, N. Söger, M. Pfeifer, Y. Demel, L. Mussmann, Appl. Catal. B: Environ. 67 (2006) 187-196.

[53]. M. Koebel, G. Madia, M. Elsener, Catal. Today 73 (2002) 239-247.

[54]. S. Roy, B. Viswanath, M.S. Hegde, G. Madras, J. Phys. Chem. C 112 (2008)

6002-6012.

[55]. R.Q. Long, R.T. Yang, J. Catal. 198 (2001) 20-28.

[56]. H.Y. Huang, R.Q. Long, R.T. Yang, Appl. Catal. A: Gen. 235 (2002) 241-251.

[57]. A. Grossale, I. Nova, E. Tronconi, D. Chatterjee, M. Weibel, J. Catal. 256(2008) 312-322.

[58]. J.H. Kwak, R. Tonkyn, D. Tran, D.H. Mei, S.J. Cho, L. Kovarik, J.H. Lee, C.H.F. Peden, J. Szanyi, ACS Catal. 2 (2012) 1432-1440.

[59]. S. Suárez, S.M. Jung, P. Avila, P. Grange, J. Blanco, Catal. Today 75 (2002) 331-338.

Tables and Figure captions:

Table 1. Fe loading, surface atom concentration and surface area of catalysts

Catalysts	Fe content* (wt%)	Surface area BET (m^2/g)	Total pore volume (mL/g)	Pore diameter (nm)
H-ZSM-5	-	425.06	0.2273	1.16237
Fe-ZSM-5	0.97	391.38	0.2154	1.13005
Fe_2O_3	77.54	112.13	-	-
Fe_H-ZSM-5	22.12	305.65	0.1542	1.0796

*Surface atomic ratio was determined by EDS.

Table 2. The area of the subbands derived by deconvolution of the TPD spectra and the UV/VIS-DRS spectra ($Area_1$ at $\lambda < 300$ nm, $Area_2$ at $300 < \lambda < 400$ nm, and $Area_3$ at $\lambda > 400$ nm)

Catalysts	Amount of acid		Existing form of Fe species		
	$Area_w$ [a]	$Area_s$ [b]	$Area_1$ [c]	$Area_2$ [d]	$Area_3$ [e]
H-ZSM-5	43.96	55.89	-	-	-
Fe-ZSM-5	27.14	29.95	73.6	16	24.6
Fe_2O_3	18.79	-	-	-	-
Fe_H-ZSM-5	31.16	15.90	60.1	37.9	110.3

[a] weak surface acid sites

[b] strong surface acid sites

[c] Isolated Fe^{3+} in tetrahedral and higher coordination.

[d] Small oligomeric Fe_xO_y clusters.

[e] Large Fe_xO_y clusters.

Fig. 1. (a) NO conversion over this series of catalysts. (b) Ea calculated using the Arrhenius plot according to equation (2) over Fe_H-ZSM-5, the inset shows the k calculated according to equation (1). The inset is the k calculated according to equation-1. Reaction conditions: 800 ppm NO, 800 ppm NH_3, and 5% O_2 balanced by N_2 at total flow rate of 1000 sccm and a GHSV of 100,000 h^{-1}.

Fig. 2. XRD patterns of the samples.

Fig. 3. Typical SEM images of (a) H-ZSM-5, (b) Fe-ZSM-5, (c) Fe_2O_3, and (d)Fe_H-ZSM-5.

Fig. 4. UV-vis spectra of Fe-ZSM-5 and Fe_H-ZSM-5.

Fig. 5. Fe_{2p} XPS spectra of H-ZSM-5, Fe-ZSM-5, Fe_2O_3, and Fe_H-ZSM-5.

Fig. 6. H_2 temperature programmed reduction profiles of catalysts.

Fig. 7. NH_3 temperature programmed desorption profiles of catalysts.

Fig. 8. Oxidation of NO to NO_2 by O_2 over the catalysts. Reaction conditions: [NO] = 800 ppm, [O_2] = 5%, balanced by N_2 at total flow rate of 1000 sccm and a GHSV of 40,000 h^{-1}.

Fig. 9. NO-TPD and NO_2-TPD profiles of the catalysts.

Fig. 10. NH_3 oxidized by O_2 over the catalysts. Reaction conditions: $[NH_3]$ = 800 ppm, $[O_2]$ = 5%, balanced by N_2 at total flow rate of 1000 sccm and a GHSV of 40,000 h^{-1}.

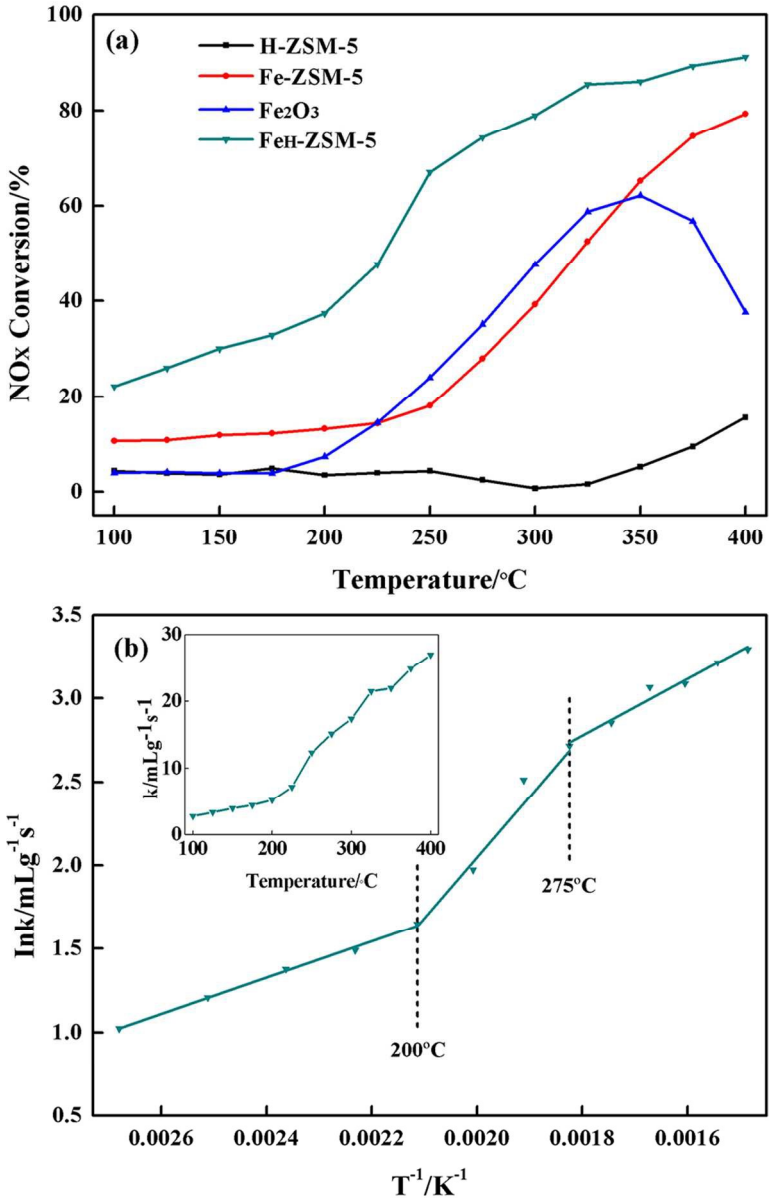

80x125mm (300 x 300 DPI)

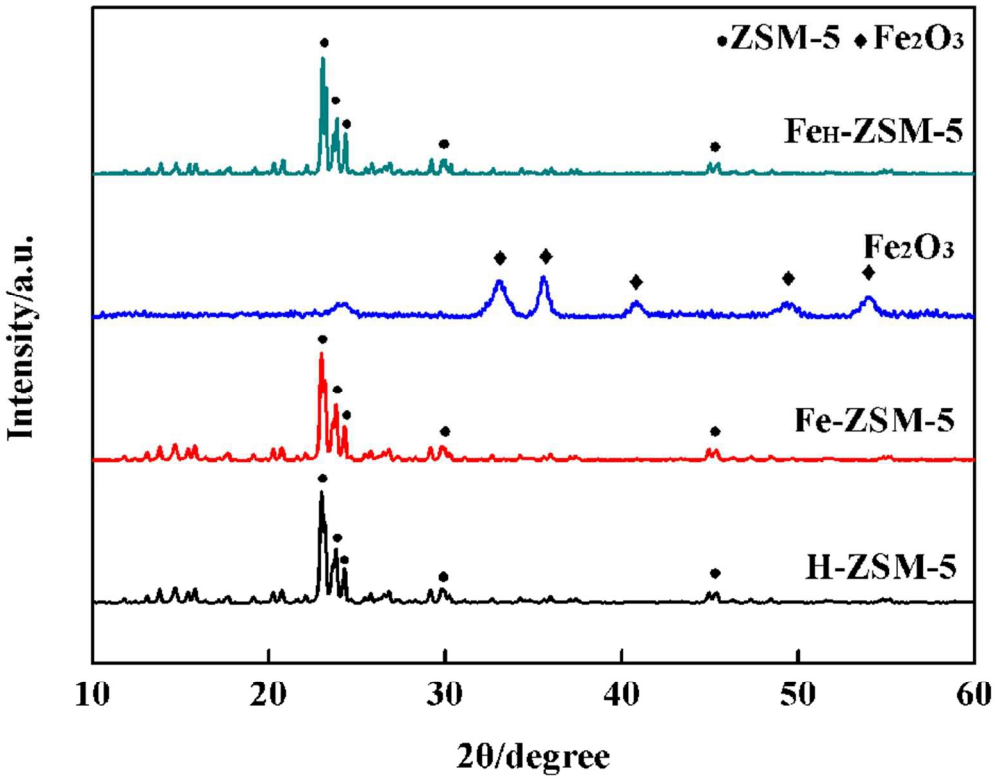

80x61mm (300 x 300 DPI)

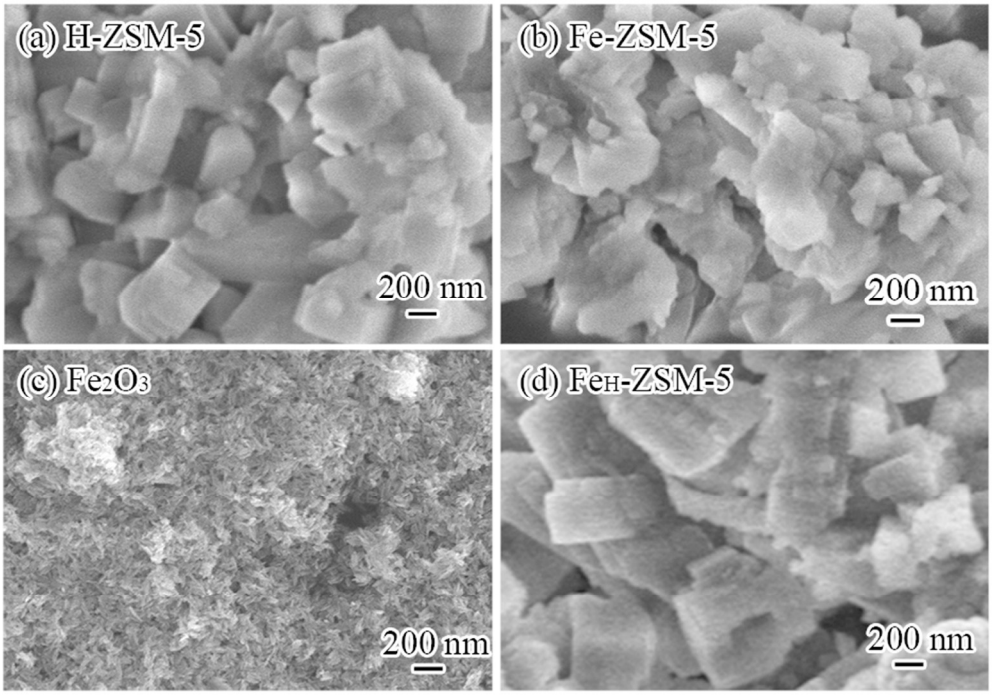

80x55mm (300 x 300 DPI)

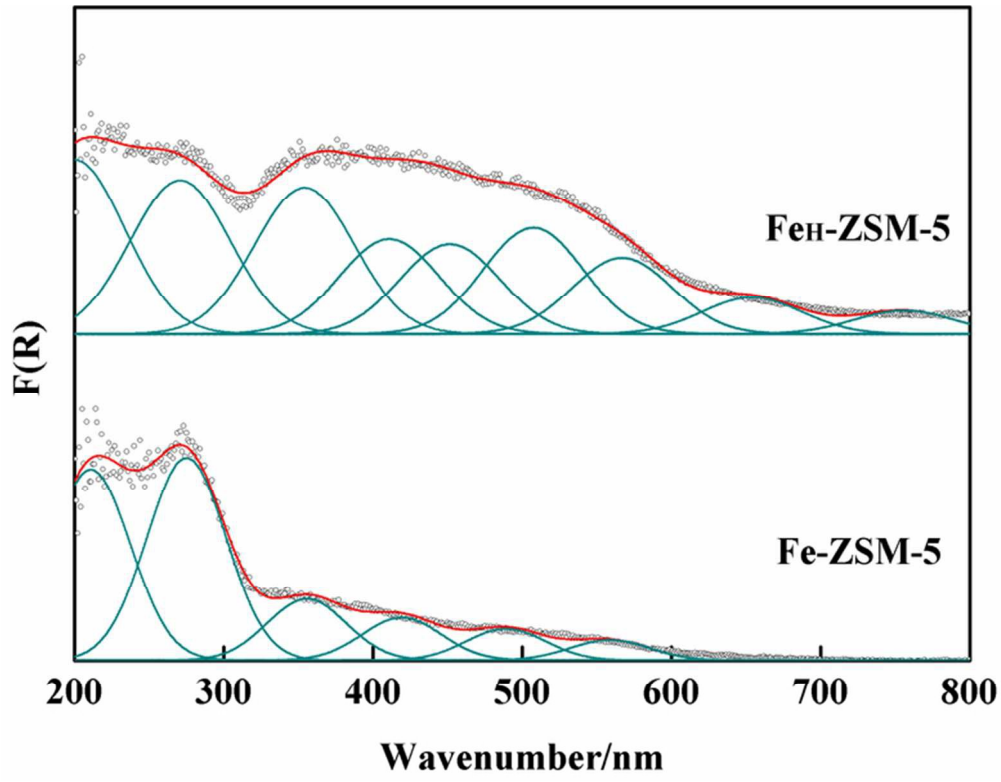

65x51mm (300 x 300 DPI)

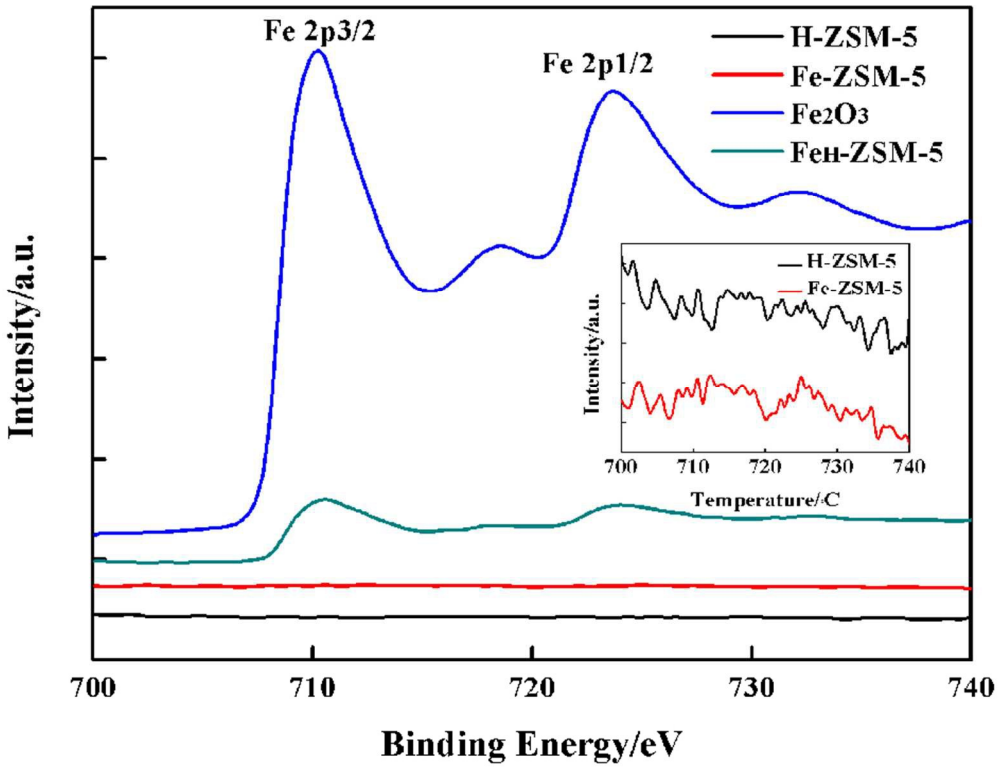

80x60mm (300 x 300 DPI)

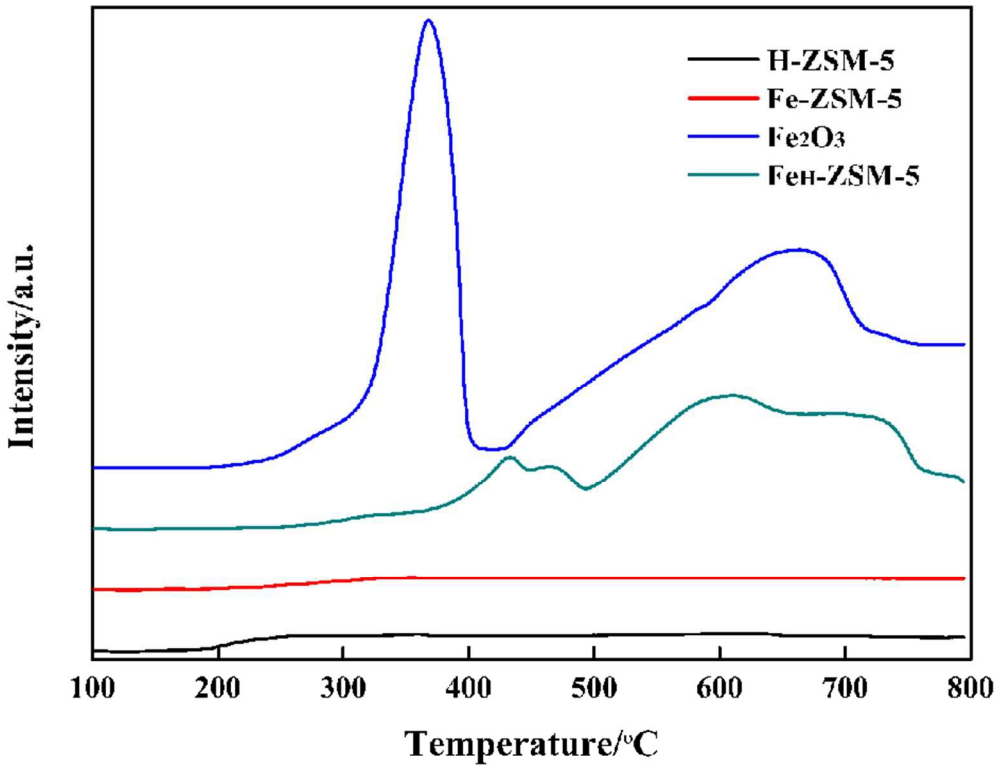

80x60mm (300 x 300 DPI)

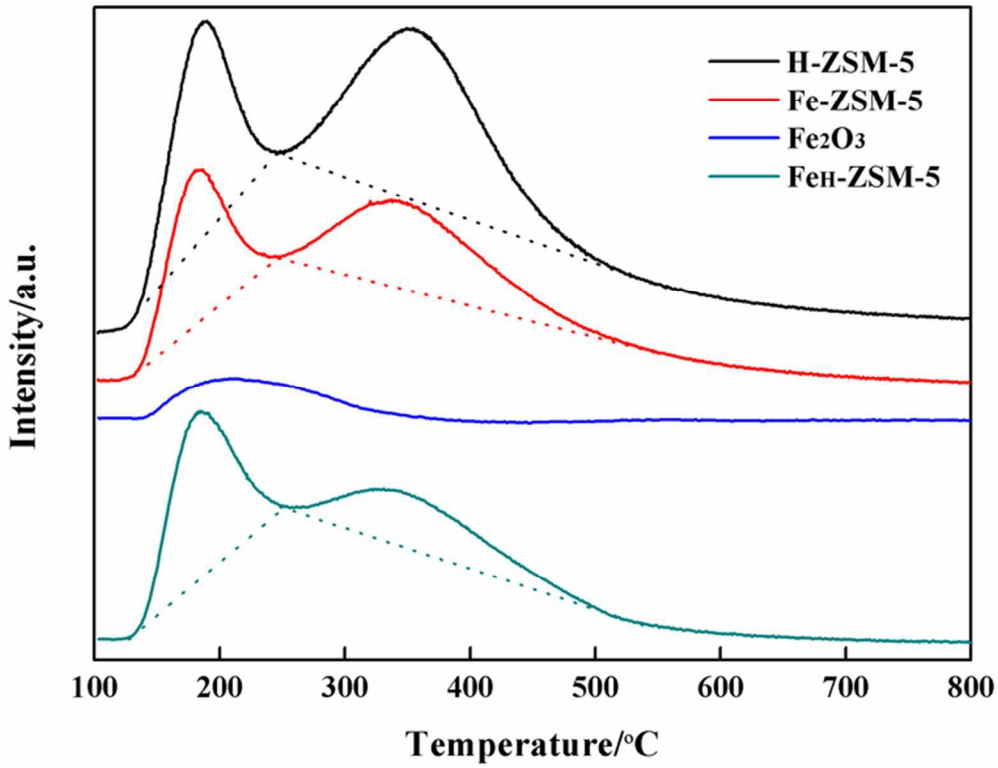

64x49mm (300 x 300 DPI)

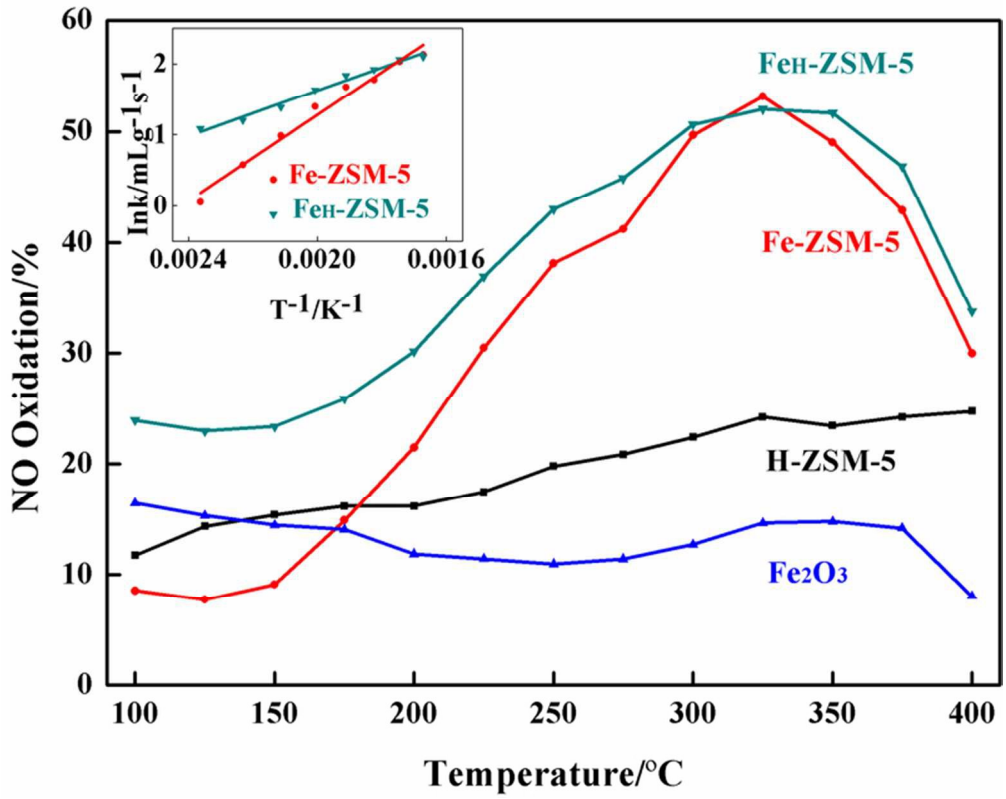

67x54mm (300 x 300 DPI)

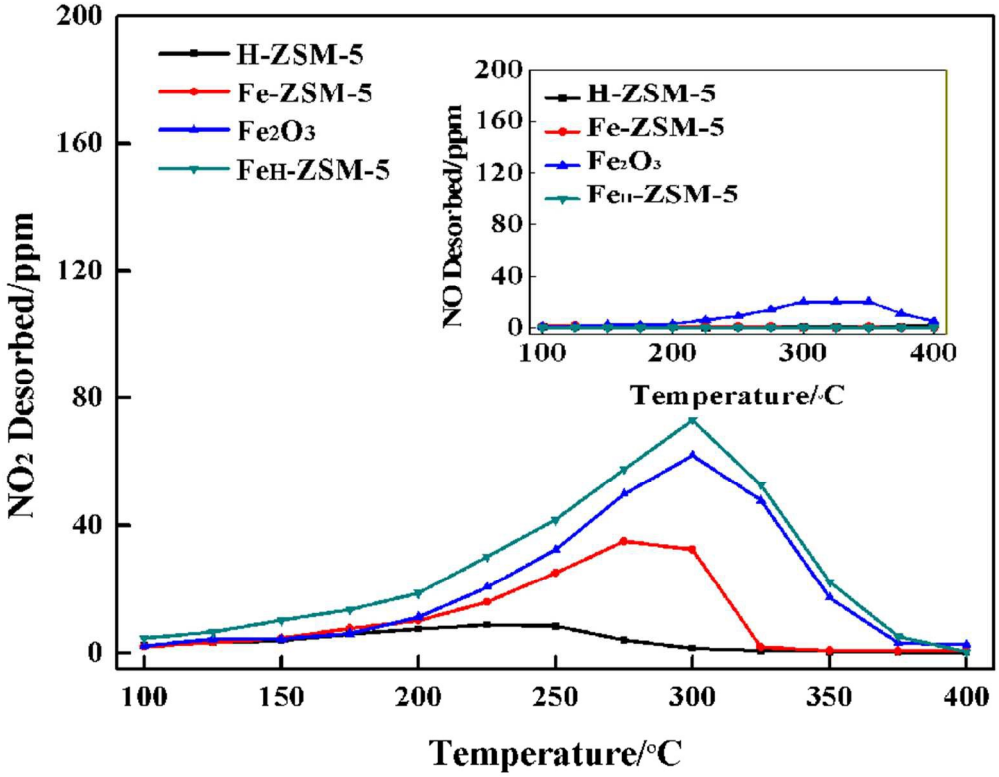

80x62mm (300 x 300 DPI)

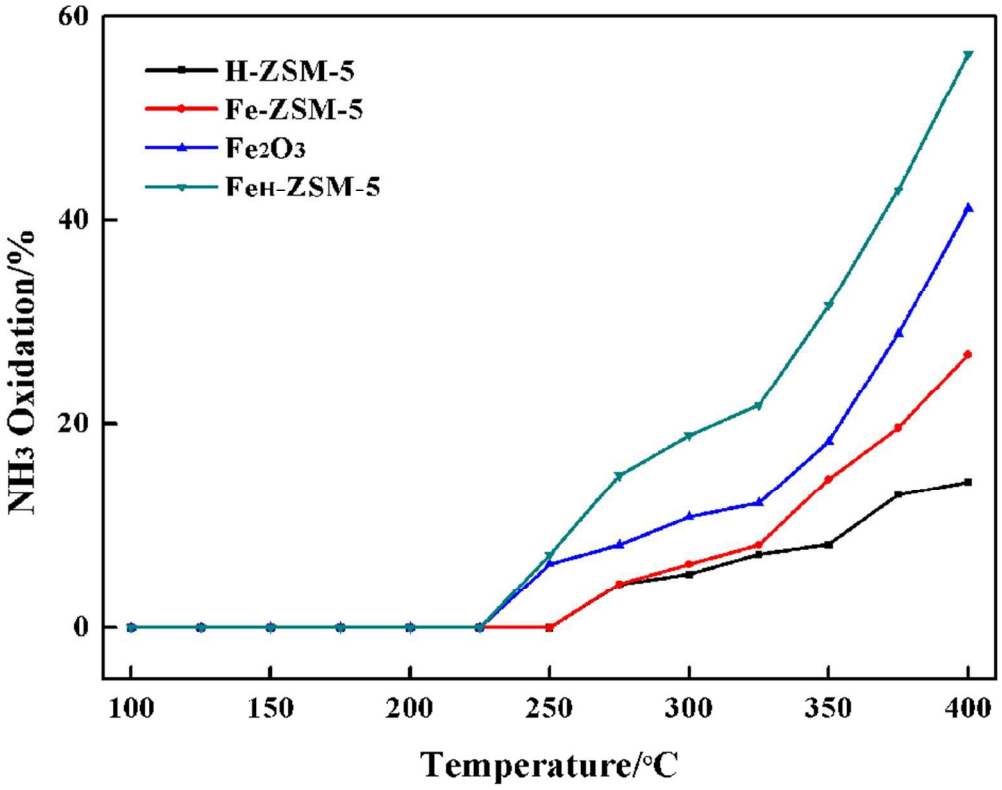

80x63mm (300 x 300 DPI)

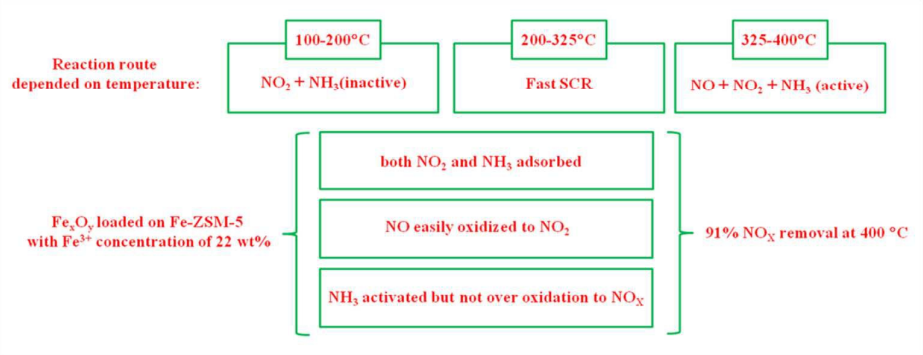

Highly dispersed Fe_xO_y clusters loaded on Fe-ZSM-5 with a Fe^{3+} concentration up to 22 wt%, the Fe_xO_y clusters promoted the de-NO_X activity with an efficiency of 91%, the reaction route was temperature dependent.